Nature Potential for COVID-19: Targeting SARS-CoV-2 M^{pro} Inhibitor with Bioactive Compound

Kaushik Kumar Bharadwaj [1], TanmaySarkar [2], Arabinda Ghosh [3], Debabrat Baishya [1], Bijuli Rabha [1], Manasa Kumar Panda [5], Bryan R. Nelson [8,9], Akbar John[10], Hassan I. Sheikh [7],Bisnu Prasad Dash [11], Hisham A. Edinur [6]* and Siddhartha Pati[4,9,]*

[1] Department of Bioengineering and Technology, Gauhati University, Guwahati- 781014, Assam, India
[2] Malda Polytechnic, West Bengal State Council of Technical Education, Govt. of West Bengal, West Bengal 732102, India
[3] Microbiology Division, Department of Botany, Gauhati University, Guwahati, Assam, India-781014
[4] Centre of Excellence, Khallikote University,Berhampur- 761008 Ganjam, Odisha, India
[5] Environment and Sustainability Department, CSIR-Institute of Minerals and Materials Technology, Bhubaneswar, India
[6] Forensic Science Programme, School of Health Sciences, University Sains Malaysia, Health Campus, KubangKerian 16150, Kelantan, Malaysia
[7] Faculty of Fisheries and Food Science, University Malaysia Terengganu, 21030, Kuala Nerus, Terengganu, Malaysia
[8] Institute of Tropical Biodiversity and Sustainable Development, University Malaysia Terengganu, Kuala Nerus 21030, Terengganu, Malaysia
[9] Research Divisions, Association for Biodiversity Conservation and Research, Devine Colony, Balasore, Odisha 756001, India
[10] INOCEM Research Station, Kulliyyah of Science, International Islamic University Malaysia, 25200 Kuantan, Pahang, Malaysia
[11] Department of Biosciences and Biotechnology, Fakir Mohan University, Balasore, India
* Correspondence: patisiddhartha@gmail.com (S.P.); edinur@usm.my (H.A.E.)

Abstract: Corona viruses were first identified in 1931 and SARS-CoV-2 is the most recent. COVID-19 is a pandemic that put most of the world on lockdown and the search for therapeutic drugs is still on-going. Therefore, this study uses *in silico* screening to identify natural bioactive compounds from fruits, herbaceous plants and marine invertebrates that are able to inhibit protease activity in SARS-CoV-2(PDB: 6LU7). We have used various screening strategies such as drug likeliness, antiviral activity value prediction, molecular docking, ADME (absorption, distribution, metabolism, and excretion), molecular dynamics (MD) simulation and MM/GBSA (molecular mechanics/generalized born and surface area continuum solvation). 17 compounds were shortlisted using Lipinski's rule. 5 compounds revealed significantly good predicted antiviral activity values and out of them only 2 compounds, Macrolactin A and Stachyflin, showed good binding energy values of -9.22 and -8.00 kcal/mol within the binding pocket, catalytic residues (HIS 41 and CYS 145) of M^{pro}. These two compounds were further analyzed for their ADME properties. The ADME evaluation of these 2 compounds suggested that they could be effective as therapeutic agents for developing drugs for clinical trials. MD simulations showed that protein-ligand complexes of Macrolactin A and Stachyflin were stable for 100 nano seconds. The MM/GBSA calculations of M^{pro} – Macrolactin A complex indicated higher binding free energy (-42.58 ± 6.35 kcal/mol) with M^{pro} protein target receptor (6LU7). DCCM and PCA analysis on the residual movement in the MD trajectories confirmed the good stability on Macrolactin A bound state of 6LU7. This signify the stable conformation of 6LU7 with high binding energy with Macrolactin A. Thus, this study showed that Macrolactin A could be an effective therapeutical agent for SARS-CoV-2protease (6LU7) inhibition. Additional *in vitro* and *in vivo* validations are needed to determine efficacy and dose of Macrolactin A in biological systems.

Keywords: Coronavirus; pandemic; communicable disease; treatment; molecular docking; MD simulation; ADMET; MM/GBSA.

1. Introduction

The 2003 SARS-CoV outbreak caused 10 % fatality [1], MERS-CoV produced 35% fatality [2] and now, SARS-CoV2 is responsible for 2.35 % fatalities [3]. The experiences gained from managing previous novel coronavirus infections in healthcare facilities were associated the lower the fatalities of SARS-CoV2 [4,5]. However, the virulence of SARS-CoV2 lead to national-based quarantine and standard operating procedures were the only feasible approach to break the chain of infections while the entire world patiently waited for an effective vaccine against SARS-CoV2 [6]. SARS-CoV2 has high RNA polymerase mutation rate that made this pathogen-resistant against antiviral drugs and thus, increases the chances of re-infection [7-8]. Experience from using lopinavir/ritonavir and remdesivir during SARS-CoV led to identical treatment measures for SARS-CoV-2, however, the efficacy of these drugs is not as expected and patients in critical conditions have slimmer chances for recovery [9, 10]. In a recent survey, the willingless to take these vaccines were affected by its halal status and cost. The study recommended that the governments should subsidize the cost [10]. For developing countries these vaccines might not be affordable. Moreover, Healthcare facilities are restricted to developed areas, while rural communities rely on herbs to treat diseases and infections. Previous studies indicated that natural products were therapeutic for coronavirus, coxsackievirus, dengue virus, enterovirus, hepatitis virus, herpes simplex virus, human immunodeficiency virus (HIV) and respiratory syncytial virus symptoms [11]. Unfortunately, technical barriers and certifications favors the use of modern medicine which led to natural compounds being gradually forgotten [12]. Recent studies showed that compounds from *Andrographis paniculate* were effective against SARS-CoV2[17]. At then end of 2020, various news outlets such as Bloomberg, the business times, and straits times reported that Thailand have approved A. paniculate's usage for patient in lower stage of Covid-19 infections. Antiviral research targets the inhibition of various virus parts such as spike proteins,

reverse transcriptase, integrase, RNA and protease enzyme (e.g. M^{pro} and $3CL^{pro}$) [13]. *In silico* identification is low-cost, efficient, brief and virtual to quantify activity relationships between target biomolecules such as DNA, RNA and proteins), and inhibitors from synthetic and natural sources during drug discovery [14, 15]. Research on SARS-CoV-2 identified 29 proteins comprising of structural, spike, envelope, membrane, nucleocapsid, non-structural and adjunct proteins. Among all, an encoding protease was determined to be responsible in the process of making about 16 of these 29 proteins [16]

The macrolactin compounds are known to have a broad range of pharmacological activities including antiviral, antitumor, antibacterial, antiangiogenic, neuro-protective, antiproliferative activities, intestinal bowel disease protecting and bone-remodeling activities [18]. The macrolactins are polyene macrolides containing a 24- membered lactone ring containing with conjugated double bonds [19]. So far, six macrolactins (A-F) have been chemically characterized, and only macrolactins A and E have been studied for total synthesis [20]. Macrolactin A showed selective antibacterial activity, inhibited B16-F10 murine melanoma cancer cells in vitro assays, showed significant inhibition of mammalian Herpes simplex viruses (types I and II), and protected T-lymphoblast cells against human HIV viral replication [19].

Briefly, it can be said that the present study aimed to identify bioactive compounds from natural aquatic and terrestrial sources using *in silico* screening via molecular docking and molecular dynamics (MD) simulations to analyze and predict the consistency of the protein-ligand complexes for selected inhibitors of SARS-CoV-2 viral protease.

2. Result and Discussion

2.1. Screening Process and Molecular Docking Analysis

Natural compounds (30) (Supplementary Table S1) with antioxidant, antimicrobial, antiviral and anticancer properties were identified from plants and animals for screening using Lipinski's rule against M^{pro} to assess the binding activity following published methods from the literature [21, 22, 23, 24]. From 30 compounds, a total of 17 compounds were possessing suitable drug-likeness properties (Supplementary Table S2). These compounds were then selected for the prediction of structure-based antiviral activity by using PASS online server. It gives a probability active (Pa Score) that ranges from 0 to 1 and a value of >0.3 can be considered as active [25]. A total of 5 compounds have predicted to possess the antiviral activity score (Pa) of 0.6 (60%) (Supplementary Table S3). These 5 compounds were further investigated for molecular docking study to explore a possible SARS-CoV2 M^{pro} inhibitor. Two compounds namely, Macrolactin A (PUBCHEM ID: 6451096), and Stachyflin (PUBCHEM ID: 493326) showed low binding energy (-9.22 to -8.00 kcal/mol) which indicated effectiveness (Supplementary Table S4). These top 2 hit inhibitory compounds with good binding energy to the selected receptor and were further analysed for ADME properties (Table 1). All the 2 compounds have shown good physico-chemical parameters where almost all the parameters were in suggested ranges, hence they were further investigated by performing MD simulations which showed Macrolactin A and Stachyflin formed a stable protein-ligand complex. Finally, MM-GBSA analysis was carried out and Macrolactin A was the best inhibitors of the M^{pro}. Various literature has reported different compounds that possess binding energy ranges from -7.0 to -8.5 kcal/mol, which might be a key to inhibit SARS-CoV2 infection [26, 27]. The overall strategies for screening naturally occurring compounds against M^{pro} are depicted in Figure 1. Presently, in our study, only Macrolactin A binds with energy of -9.22 kcal/mol to SARS-CoV-2 M^{pro}(PDB ID: 6LU7) protein was the top inhibitors of the M^{pro} having a good pharmacokinetic property and could be a treatment to SARS-CoV-2 infection.

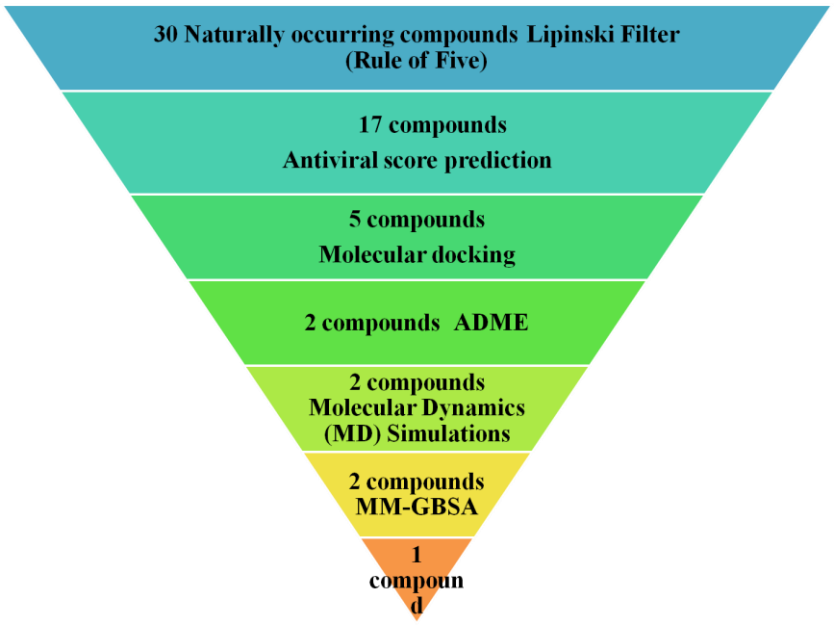

Figure 1. Virtual screening strategy of naturally occurring compounds against M^{pro} as inhibitor.

Docking interactions of these two naturally occurring compounds with the binding site residues are shown (Figures 3, 4 and Table S4). The compound Macrolactin A (Figure 2) interacted with the residues HIS 41, MET 49, PHE 140, LEU 141,

ASN 142, GLY 143, SER 144, CYS 145, HIS 163, HIS 164, MET 165, GLU 166, ARG 188, and GLN 189 in the binding site of M^{pro} to form the docking complex (Figure 3). The Macrolactin A compound showed good binding affinity(-9.22 kcal/mol) with 0.175 µM, forming 3 hydrogen bonds, 9 Van der Wall's interactions, hydrophobic interactions, carbon-hydrogen bond and alkyl interactions (Figure 3). Stachyflin (Figure 2) also showed good binding affinity (-8.00 kcal/mol) with 1.37 µM with the residues THR 25, LEU 27, HIS 41, MET 49, LEU 141, ASN 142, GLY 143, SER 144, CYS 145, HIS 163, HIS 164, MET 165, GLU 166, ARG 188, and GLN 189 of M^{pro} active site. Stachyflin formed two hydrogen bonds, 9 Van der Wall's interactions, hydrophobic interactions, π donor-hydrogen bonds, alkyl and π-Alkyl interactions (Figure 4). This result was in agreement with a previously published report that candidate and lead compounds formed the highest number of hydrogen with GLU 166 [28].

Previous studies also showed that natural compounds can interact with the catalytic site of M^{pro} proteases at HIS41 and CYS145 [24, 29]. Previous research indicated that binding energy of -7.0 kcal/mol or less could be effective against SARS-CoV-2 which causes COVID-19 [26]. Previous studies reported that the inhibitor N3 docks in the active binding site of 6LU7 and forms hydrogen bonds with THR190, GLN189, GLU166, HIS 164, PHE 140, and GLY 143 [30]. As mentioned previously, Thailand approved the use of *A. paniculate* for mild Covid-19 cases. Phytochemicals from *A. paniculate* also formed hydrophobic interactions and hydrogen bonding interactions with different residues THR24 to GLN192[17]. The binding energy of co-crystallized N3 inhibitor was previously reported to be −7.6 kcal/mol [28]. The biding energy of andrographolide (-6.26 kcal/mol) and dihydroxy dimethoxy flavone (− 6.23 kcal/mol) from A. paniculate were better compared to hydroxychloroquine (-5.47 kcal/mol) [17]. Amentoflavone, a natural compound synthesized by plants, formed 3 hydrogen bonds and numerous hydrophobic interactions with 6LU7 had binding energy of -10.2 kcal/mol in a previous study [28]. Although all the three compounds showed comparatively good binding energies, the physicochemical properties and stability of the docking complexes needed to be tested.

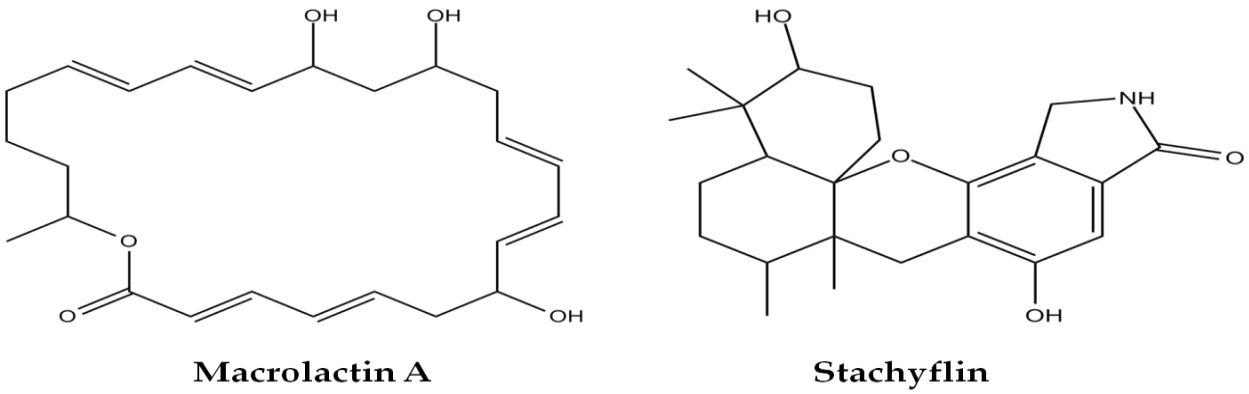

Figure 2. 2D structures of top two selected hit compounds that required the lowest binding energies during the protein-ligand formation.

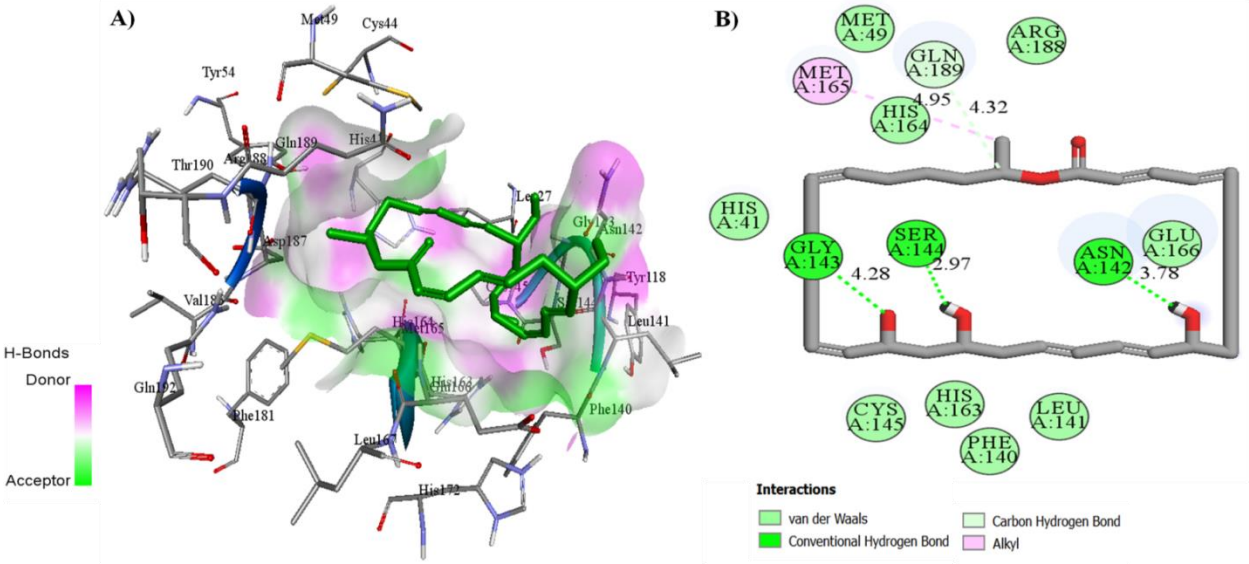

Figure 3. Molecular docking displaying the interaction of Macrolactin A with 6LU7 protein. (**A**) 3D ligand interaction representing the docked pose in the binding site (**B**) 2D plot of the ligand interaction with the amino acids residues.

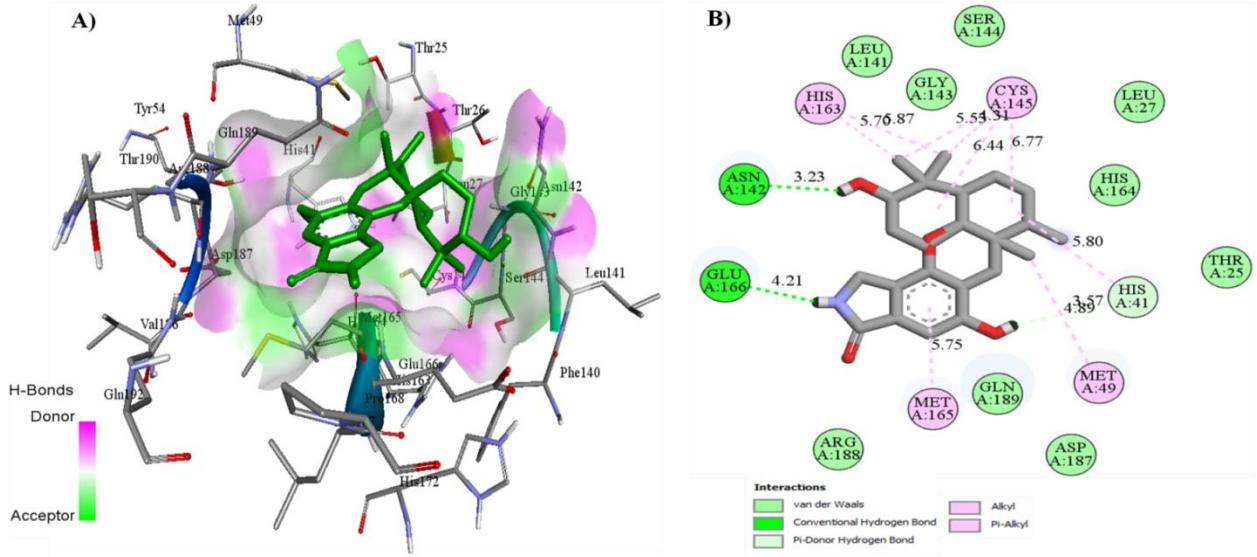

Figure 4. Molecular docking interaction of Stachyflin with 6LU7 protein. (**A**) 3D ligand interaction representing the docked pose in the binding site (**B**) 2D plot of the ligand interaction with the amino acids residues.

2.2. ADME Properties Analysis

Evaluations of physicochemical properties via ADME analysis are essential for assessing the efficacy of potential drug candidates and predict the drug-likeness properties. The calculated ADME properties and predicted physicochemical properties of the two-hit compounds are given in Table 1. All the analyzed parameters of the three top compounds were in the recommended range. Although some compounds showed higher % of Human oral absorption the drug-likeness score (# star) of both the compounds were in the recommended range except % Human oral Absorption and dipole moment. Macrolactin A(94.59%) which was the best compound however, further derivatization in molecular structure could improve pharmacokinetic descriptors generally. Previous studies showed that the percentage of human oral absorption of andrographolide (77.65%) and dihydroxy dimethoxy flavone (93.829%) from *A. paniculate* were better compared to hydroxychloroquine (93.21%)[17].

Table 1. ADME prediction of Macrolactin A and Stachyflin.

Properties and functions	Predictive results		Recommended range
	Macrolactin a	Stachyflin	
Mol. Wt. (Da)	402.53	385.502	130–725
#Stars	1	0	0–5
SASA	710.02	592.553	300–1000
Dipole	0	0	1.0–12.5
Donor H-bond	3	3	0–6.0
Acceptor H-bond	7.1	5.7	2.0–20.0
QPlogPo/w	3.704	2.619	-2-6.5
QPlogS	3.062	-4.597	-6.5–0.5
QPlogkhsa	0	0.47	-3-1.2
QPlogBB	-2.125	-1.02	-3.0-1.2
No. of Metabolites	6	4	1–8
% Human oral Absorption	94.59	84.45	> 80% is high < 25% is poor

2.3. Molecular Dynamics (MD) Simulation

The MD simulation (MDS) was performed for M^{pro}-Macrolactin A, and M^{pro}-Stachyflin docking complex with 100ns simulation time and results were analysed for Root mean square deviation (RMSD), Root mean square fluctuation (RMSF), and the number of hydrogen bonding. RMSD calculation of M^{pro}-Macrolactin A complex is more stable throughout simulation as compared to the M^{pro}-Stachyflin docking complex (Figure 6). The compound Macrolactin A showed RMSD values between 2 to 3 Å with an average value of 2.8 Å However, the compound Stachyflin showed RMSD value between 2 to 3.5 Å with an average of 3.06 Å. The overall RMSD of the compound Macrolactin A throughout the 100ns of simulation remained uniform and hence these results confirmed the stability of the protein-ligand complex. While in case of Stachyflin slight increase in the RMSD value was observed after 50ns of simulation which increases up to 4 Å. This shows the less stability of the protein-ligand complex. This study supports the finding as previously reported [26, 30]. RMSF results revealed the Cα of M^{pro} bound

to Macrolactin A has an average RMSF value of 1.48 Å which depicted less fluctuations in the complex structure (Figure 7). Though, residues GLY 23 (1.71Å), LEU 50 (3.69Å), SER 139 (1.76Å), ASN 142 (1.81Å), ARG 222 (2.02Å), ASP 245 (1.81Å), GLY 278 (2.40Å), and CYS 300 (2.94Å) have shown slight fluctuations of residues in the Macrolactin A-M^{pro} complex during the simulation. While, in case of Stachyflin bound Cα of M^{pro} exhibited RMSF value of 1.77 Å, which is higher than M^{pro} bound Macrolactin A. The residues GLY 23 (1.5Å), ASP 48 (3.48 Å), GLN 127 (2.24 Å), TYR 154 (2.60Å), THR 169 (3.22 Å), GLY 278 (2.85Å) exhibit higher fluctuations during simulations. Interactions of hydrogen bonds between ligands (Macrolactin A and Stachyflin) and M^{pro} through the 100 ns of MD simulations were evaluated (Figure 8). Analysis of the results showed that the compound Macrolactin A formed 3 hydrogen bonds in average, during 100 ns of simulation with the M^{pro}. On the other hand, Stachyflin formed 1 hydrogen bond. This result confirmed the strong inhibition of M^{pro} by the Macrolactin A compound in the MD system and also showed similar to molecular docking results of 3 hydrogen bonding within active site residues in Mpro protein. Hence, MD simulation analysis of Mpro-Macrolactin A complex and Mpro-Stachyflin showed better binding interaction in the pocket of M^{pro}. The protein-ligand total contacts timeline diagram is prepared to study the intermolecular interactions between M^{pro} residues and Macrolactin A compound (Figure 9 (A)) after performing 100 ns of MD simulation. The top panel showed a maximum of 9 specific contacts formed between the protein and the ligand over the course of simulations and the bottom panel shows that the residues, ASN 142, TYR 154, GLU 166, and GLN 189 showed crucial interactions with the ligand which is represented by a darker shade. On the other hand, Stachyflin formed a maximum of 6 numbers of contacts with only GLU 166 as significant contacts (Figure 9 (B)). Thus we may conclude that the compound Macrolactin A are successful in making good interactions with the binding site residues of M^{pro} then Stachyflin and are involved in the stabilizations in the complex. M^{pro} protein interactions with the ligand Macrolactin A and Stachyflin were plotted as stacked bar chart plot (Figure 10), which was mainly categorized into four types: hydrogen bonds, hydrophobic, ionic and water bridges. In case of Macrolactin A -M^{pro} protein complex, water bridges plays followed by hydrogen bonds and hydrophobic interactions play a very important role in interactions. The amino acids ASN 142, GLU 166 and GLN 189 exhibited hydrogen bond contact with the protein. While in case of Stachyflin the amino acids LEU50 and GLU166 form hydrogen bond interactions. This indicated that the Macrolactin A -M^{pro} protein complex was stable throughout the simulation time. The conformational strains that might destabilize the complex were studied via ligand torsions dynamics and detailed information was obtained. The ligand torsions dynamics for the rotatable bonds present in the Macrolactin A compound are plotted in Figure. 11, while for Stachyflin they were added to Supplementary Figure S1. The plot showed the simulation trajectory of the ligand from 0.00 to 100 ns and the conformational evolution of rotatable bonds (RB). Rotatable bonds torsions were plotted in 2D and the bonds were color-coded. Dial plots showed the conformation of the torsion throughout the simulation. The beginning of the simulation is plotted in the center of the radial plot, while the time evolution is plotted radially outwards. The probability density of the torsions showed in bar plots that summarized the information obtained from the dial plots. The values on the left Y-axis of the charts are expressed in kcal/mol. The compound Macrolactin A in total showed 20 rotatable bonds and the dial plots clearly showed that the rotatable bonds rotate around -180° to 180°. Whereas, in Stachyflin only two rotatable bonds are observed. This showed that the ligand Macrolactin A has more flexibility to bind and maintain a stable conformation in the active site residue of the protein.

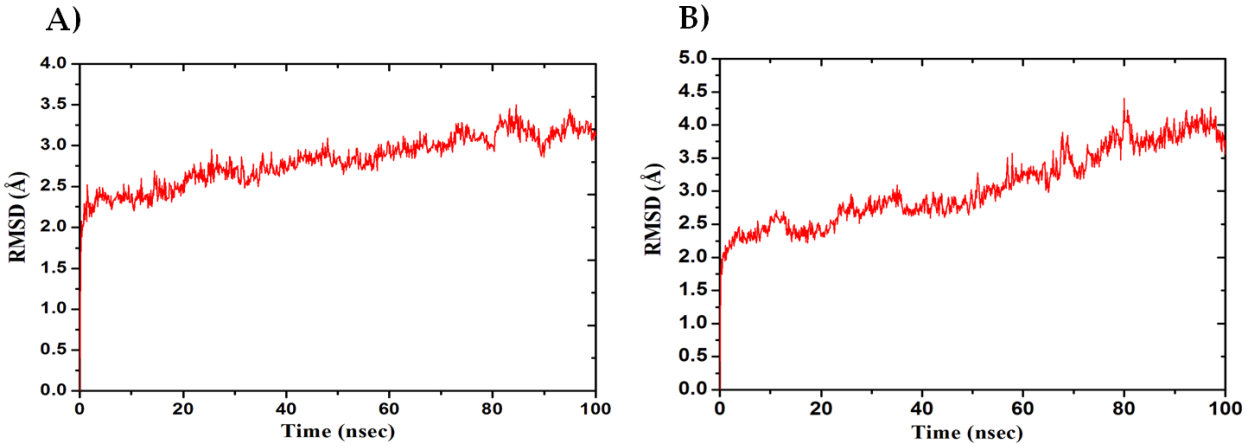

Figure 6. Plot of RMSD values, during 100ns MD simulation of M^{pro} in complex with (**A**) Macrolactin A and (**B**) Stachyflin.

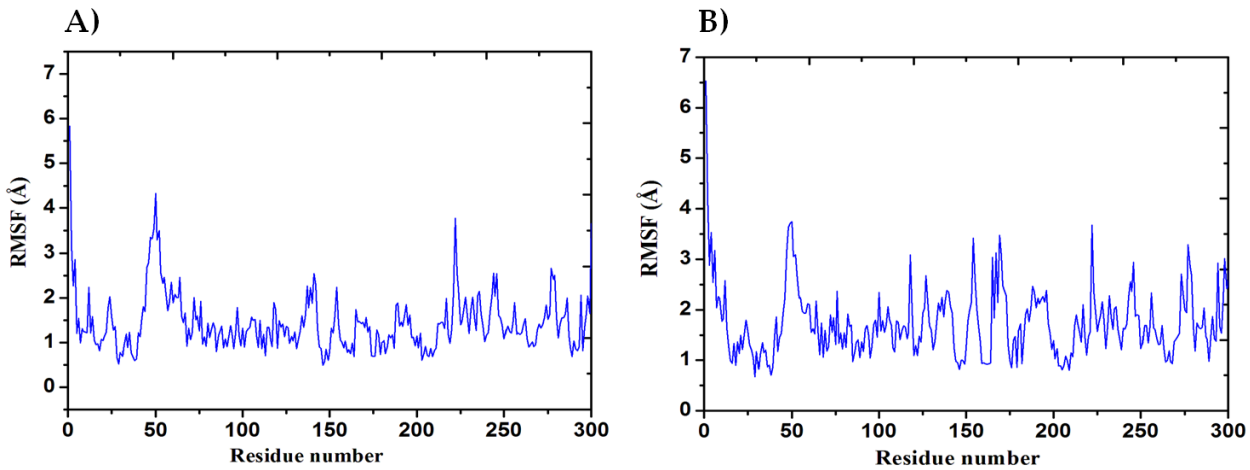

Figure 7. Plot of RMSF values, during 100ns MD simulation of M^{pro} in complex with (**A**) Macrolactin A and (**B**) Stachyflin.

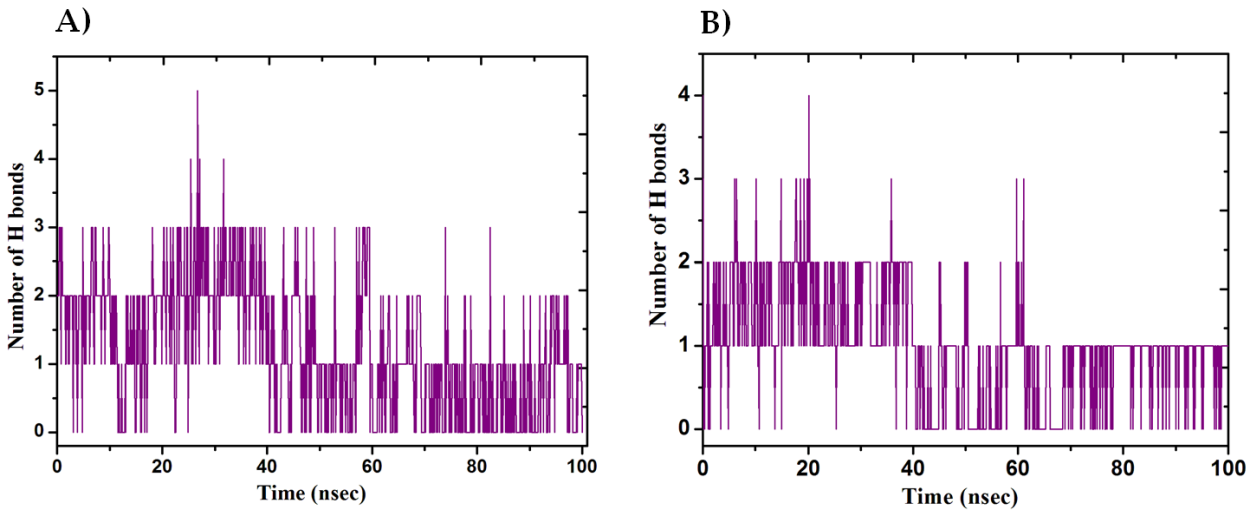

Figure 8. Plot of Hydrogen bonding interactions, during 100ns MD simulation of M^{pro} in complex with (**A**) Macrolactin A and (**B**) Stachyflin.

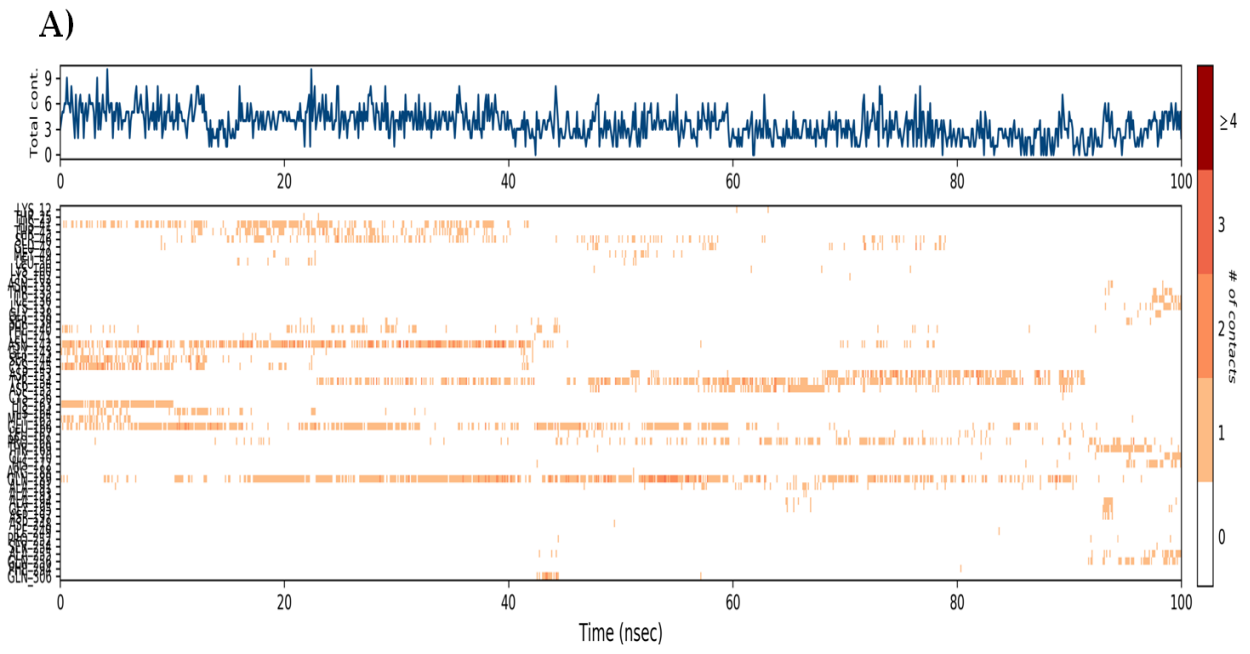

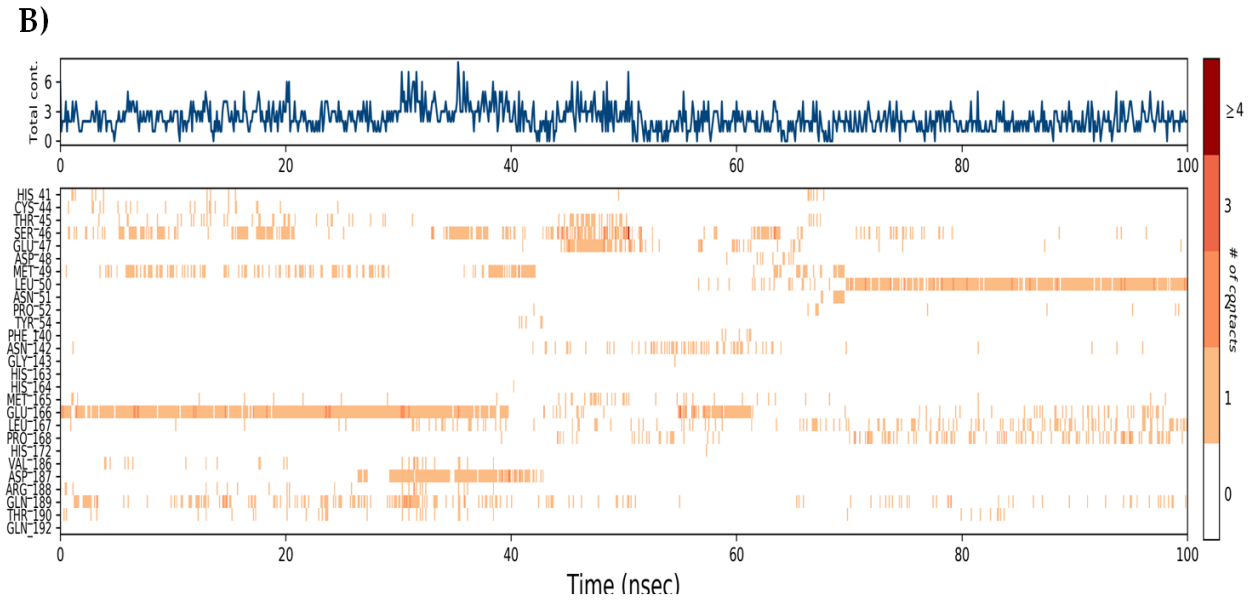

Figure 9. Analysis of total contacts timeline formed between M^{pro} residues and (A) Macrolactin A and (B) Stachyflin during MD simulation. Darker shades correspond to a higher number of contacts.

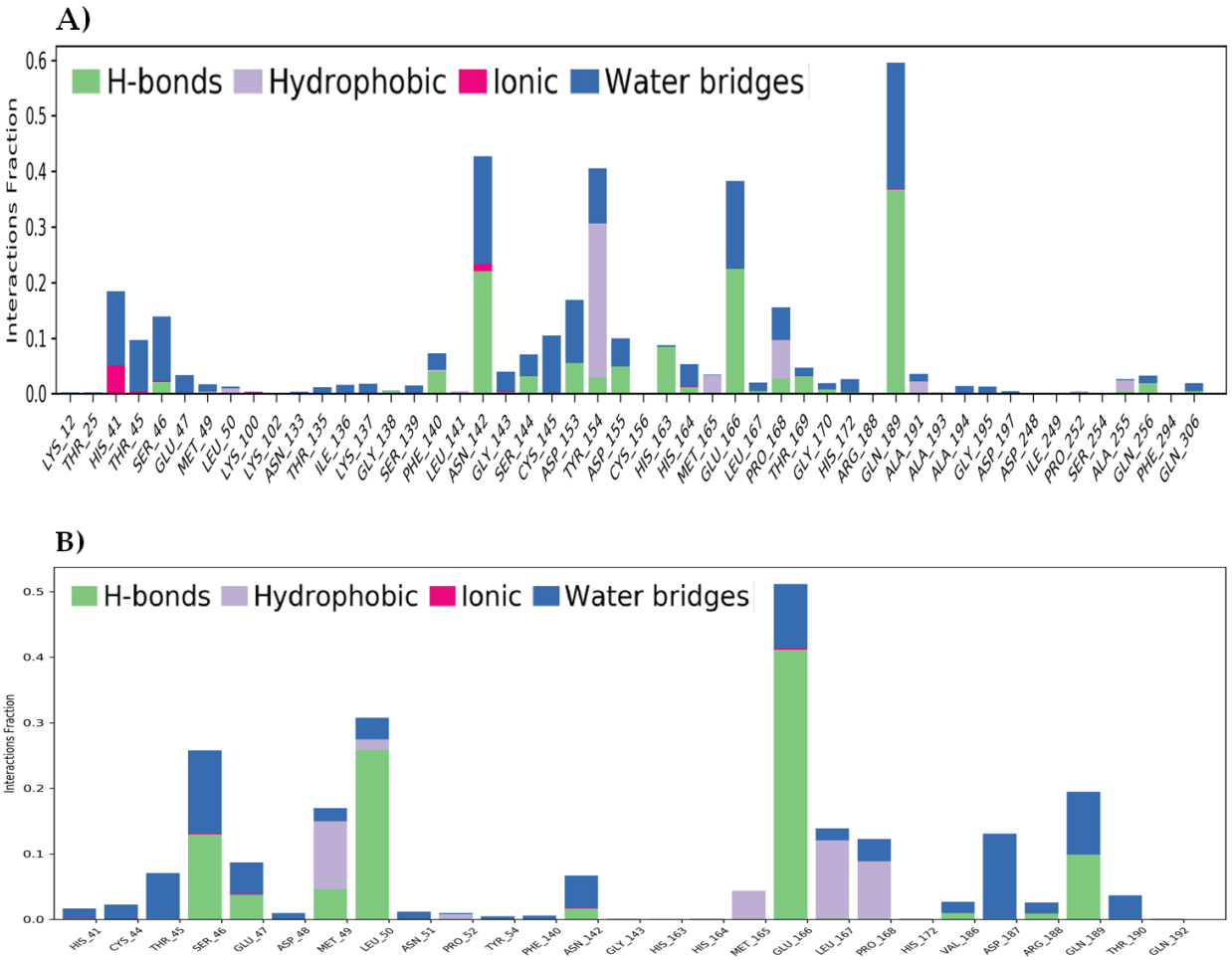

Figure 10. Protein–Ligand stacked bar chart plot of the interactions formed between ligand and protein residues during 100ns MD simulation of M^{pro} in complex with (**A**) Macrolactin A and (**B**) Stachyflin.

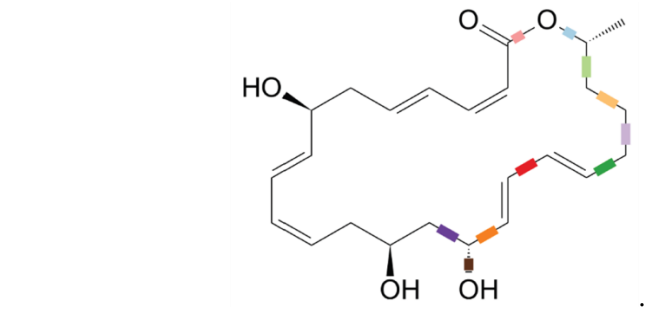

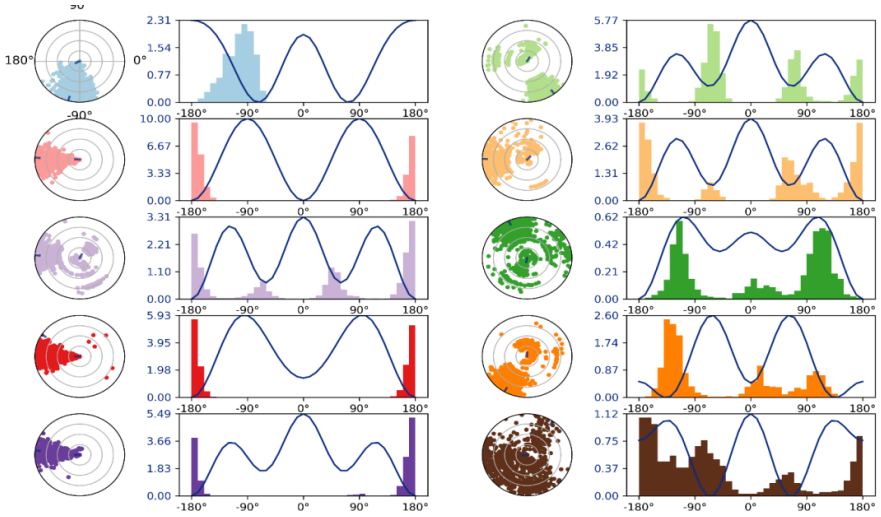

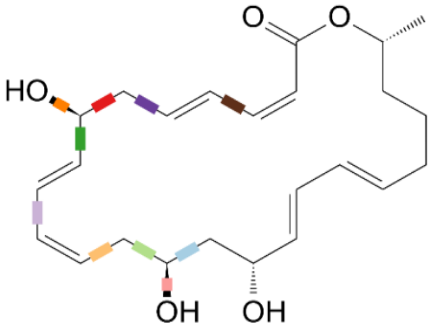

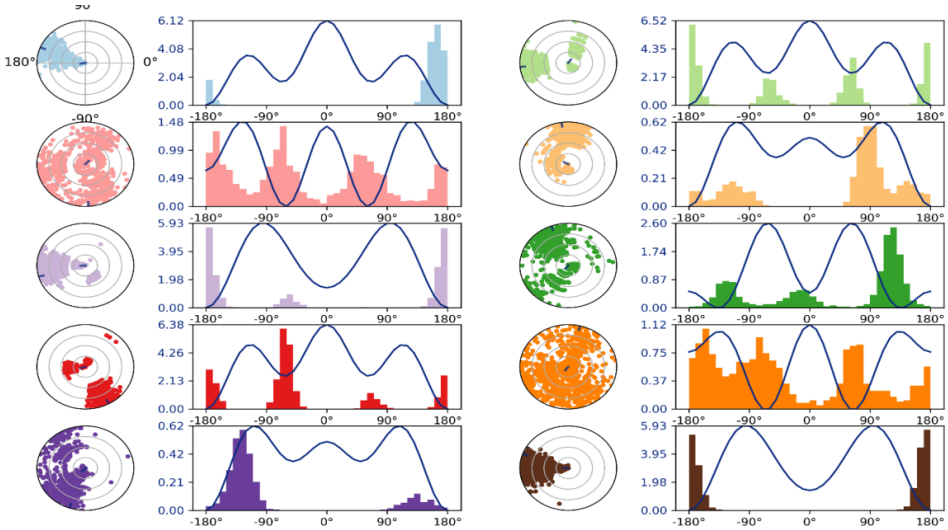

Figure 11. Analysis of rotatable bonds present in the Macrolactin A during 100ns of MD simulation.

2.4. Molecular Mechanics Generalized Born Surface Area (MM-GBSA) Calculations

Utilizing the MD simulation trajectory, the binding free energy along with other contributing energy in form of MM-GBSA were determined for each M^{pro} (PDB ID: 6LU7) complex with the 2 ligands. The results (Table 2) suggested that the maximum contribution to ΔG_{bind} in the stability of the simulated complexes were due to ΔG_{bind}Coulomb, ΔG_{bind}vdW and ΔG_{bind}Lipo, while, ΔG_{bind}Covalent and ΔG_{bind}SolvGB contributed to the instability of the corresponding complexes. The M^{pro}-Macrolactin A docked complexes showed comparatively higher binding free energy compared to other docking complexes of SARS CoV-2 M^{pro}-Stachyflin. These results supported the potential of screened compounds in inhibiting M^{pro}, showed the efficiency in binding to the selected protein and the ability to form stable protein-ligand complexes.

Table 2. Binding free energy components for the docking complexes of 6LU7 protein with ligands calculated by MM-GBSA analysis.

Compound code	MM-GBSA (kcal/mol)					
	ΔG_{bind}	**ΔG_{bind}Lipo**	**ΔG_{bind}vdW**	**ΔG_{bind}Coulomb**	**ΔG_{bind}SolvGB**	**ΔG_{bind}Covalent**
Macrolactin a	-42.58 ± 6.35	-12.24 ± 1.23	-36.13 ± 2.17	-13.83 ± 5.54	19.73 ± 2.78	2.97 ± 1.90
Stachyflin	-38.35 ± 8.40	-11.65 ± 2.08	-29.78 ± 6.17	-13.31 ± 8.69	16.30 ± 7.42	1.83 ± 1.28

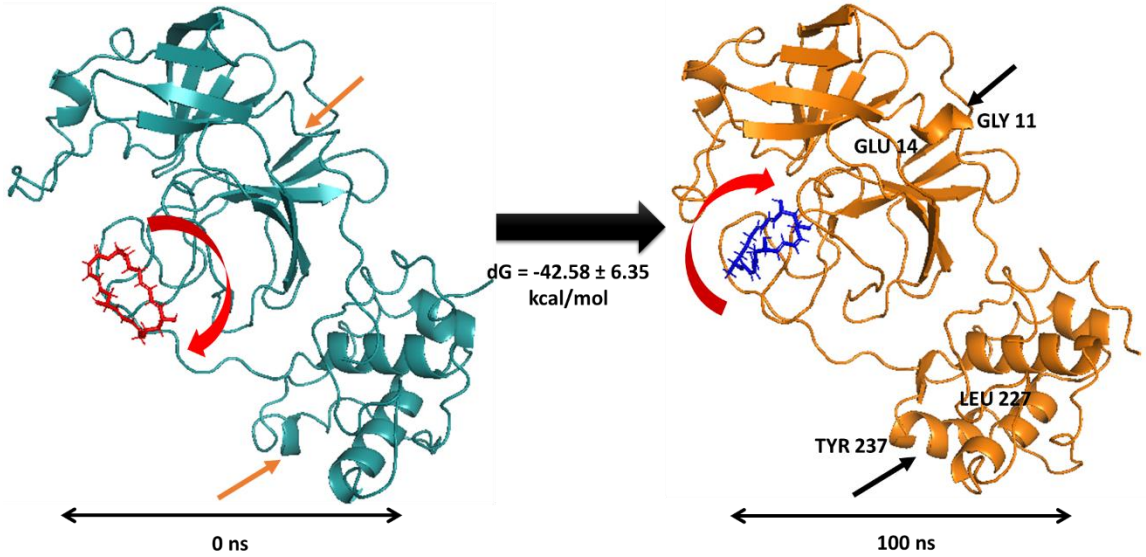

Figure 12. Position and movement of Macrolactin A at the binding site before simulation (red, 0 ns) and after simulation (blue, 100 ns). Conformational variances between first and last frame of MD simulation trajectories after 100 ns.

The analysis of the trajectories of the first and the last frame of displayed significant differences in the conformation of Macrolactin A bound 6LU7 (Figure. 12). It was observed that at the beginning of the simulation, the ligand Macrolactin A was outward from the binding site (Figure 11, red, 0 ns) whereas, at the final stage of 100 ns simulation, the ligand moved more inside the binding cavity (Figure 12, blue, 100 ns). Apart from the movement of the ligand (around 270^{0} rotation) toward binding cavity and stable fitting, that conformed into more stabilized helical turn at GLY11-GLU14 and LEU227-TYR237 in 6LU7. These conformational variances were absent before simulation and visibly clear from the last trajectory of 100 ns dynamics.

2.5. Dynamic Cross-Correlation Matrix (DCCM) and Principal Component Analysis (PCA) of the MD Simulation Trajectories

DCCM was generated in order to analyze the correlative motion of structural domains to attain a stable conformation of 6LU7 after Macrolactin A binding from MD trajectories (Figure 13A). The correlation scores on the central mean line (blue) displayed four distinct blocks having a high correlation of movement of amino acids in 6LU7 (Figure 13A). The domain D1 comprised of residues 61-90 conforming into three distinct β-sheets and extended loop (green, Figure 13B). Whereas, D2 domain having the highest cross-correlation between residues 95-165 conforming into more flexible extended loops and four β-sheets (red, Figure 13B). While D3 and D4 domains conforming into α-helices from 245-265 (cyan) and 270-280 (purple) residues, respectively. Therefore, dynamics cross correlation matrix enables the domain conformations into better stability of 6LU7 at Macrolactin A bound state. DCCM analysis also corroborates with the RMSF of C-α backbone of 6LU7 (discussed in the previous section) of Macrolactin A bound state with moderate to less fluctuations of respective amino acid residues confirming good stable structure. Similarly, Piao and coworkers (2019) reported the domain conformation and stability of N-PDZ and E-PBM proteins by their correlation function from DCCM analysis [31].

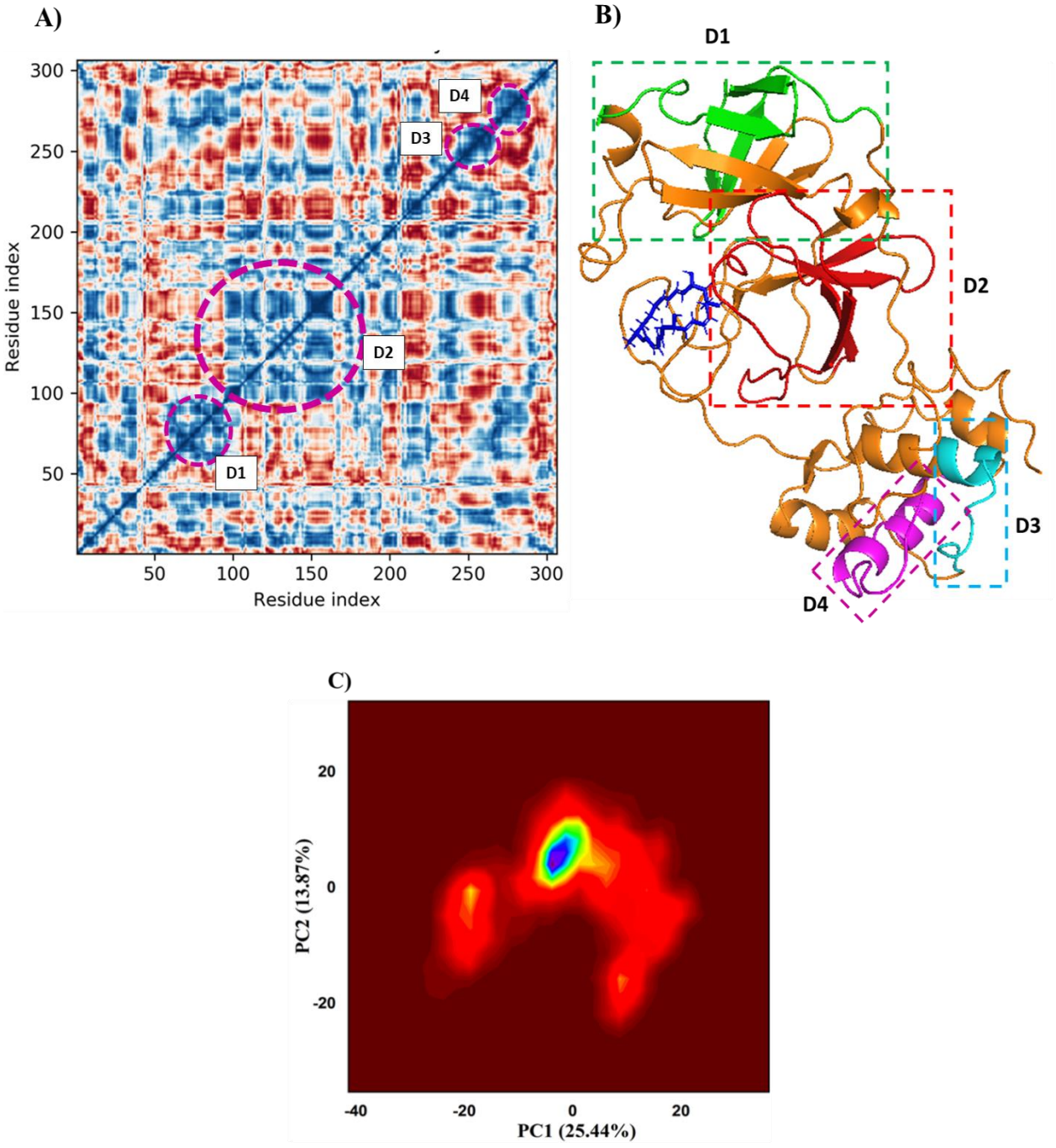

Figure 13. DCCM plot (**A**), highly correlated dynamic domains of 6LU7 (**B**) and PCA (**C**) of global (PC1) and local motion (PC2) components of 6LU7 at Macrolactin bound A state from MD trajectories.

PCA analysis displayed the contribution of principal dynamic global motion (PC1) and local motion (PC2) from the MD trajectories of 6LU7 with Macrolactin A bound complex (Figure 13C). The eigenvalues (covariance) were plotted in the PCA contour plot indicated the motion magnitude as well as directions of residues in MD trajectories. It was observed that Macrolactin A bound 6LU7 showed large movement toward positive eigenvectors and the majority of the domain movements were contributed by global slow motion (PC1) and conforming into the more stable conformation of 6LU7 depicting the significant binding of Macrolactin A thus corroborating MMGBSA result. Therefore, it may be suggested that Macrolactin A binds strongly and giving a stable conformation of C-α backbone of 6LU7.

3. Materials and Methods

3.1. Drug Likeness Profilling of Selected Natural Compounds

Virtual screening of the naturally occurring compounds (n = 30) for drug likeliness properties were performed in accordance with Lipinski's rule of five [32]. The DruLiTo stand-alone software (http://www.niper.gov.in/pi_dev_tools/DruLiToWeb/DruLiTo_index.html) is implemented for the drug-likeness screening [33]. The compounds were selected from literature based on effective cost, sustainable harvest and year-round availability in India (Table S1). The drug-likeness compounds were then predicted for antiviral activity by *in silico* using the PASS online server (http://www.pharmaexpert.ru/passonline/predict.php). The predicted antiviral activity score (Pa) ranges between 0 to 1, where the value 1 is considered as the best antiviral activity, and zero stand for no antiviral activity (Table S4). The ADME properties of the selected lead compounds were calculated by using a QikProp module in Schrodinger suite [34, 35]. Results from ADME properties like SASA, QPlogPo/w, QPlogS, QPlogkhsa, QplogBB, No. of Metabolites and % human oral absorption were compared with a recommended range of values provided in the manual. The QikProp generates descriptors which use them to perform ADMET predictions or drug-likeness parameter (indicated by # stars). The #stars parameter describes the QikProp pharmacokinetic properties that fall outside the optimum range of values for 95% of known drugs within the ConMedNP library [36, 37, 38].

3.2. Preparation of Ligands and Receptors

The Ligand was prepared using the LigPrep tool in Maestro module of Schrodinger [39, 40]. Epik was selected and Optimized Potential Liquid Simulations (OPLS3)force field [41], (pH 7.0 ± 2.0, allow 32 stereoisomers per ligand) was applied for optimization and energy minimization for each ligand compound. The receptor protein crystal structures in PDB format of the Mpro (PDB ID: 6LU7, Resolution: 2.16 Å)were obtained from the Protein Data Bank (www.pdb.org) [42]. The PDB structure and the protein–ligand structures were prepared using the Protein Preparation Wizard in the Schrödinger suite [40]. The water molecules in all protein structures were deleted before the missing residues and side chains were corrected using a Prime module [43]. The protein and the protein-ligand complexes are subjected to geometry refinement using OPLS2005 force field.

3.3. Molecular Docking

The crystal structure of M^{pro} (PDB ID: 6LU7) was used for molecular docking studies. All the protein-ligand docking complexes were performed using Autodock 4.2 [44, 45, 46]. The catalytic site of Mpro (His41 and Cys145), were chosen as binding sites for docking analysis [42].

In our docking study protein are kept rigid and ligands were kept flexible. Polar hydrogen and gasteiger charges were added to the Mpro protein (M^{pro}) and natural compound structures (ligand). AutoDock Tools (v.1.5.6) of the MGL software package was used to prepare PDBQT files of the ligands and proteins. Lamarckian Genetic Algorithm (LGA) method was used to analyze the protein-ligand docking complexes. The grid box size was set to 22.5 Å, with a grid point spacing of 0.375Å, centered on x =-13.01, y =18.361, and z = 71.031Å. The binding interactions of the docking complexes were analyzed and its 3D and 2D interaction plot were analyzed by using Discovery studio visualizer [47]. Only molecular docking complexes with the least binding were considered for further study.

3.4. MD Simulations

The top inhibitory compounds Macrolactin A and Stachyflin were further analyzed by molecular dynamics simulation under Linux environment using the Desmond modules of the Schrodinger [48, 49]. The SPC (simple point charge) water box solvent model was used and OPLS2005 force field was applied for the protein-ligand docking complexes. An orthorhombic periodic boundary box (X, Y, and Z-axis) conditions were set up at 10 Å distances to specify the shape and size of the protein-ligand docking complex. Counter ions (14 Na^+, and 18 Cl^- ions) were added to neutralize charges. 0.15M NaCl salt concentrations were added to make the system close to mimic the human physiological condition. The MD simulation was operating for 100 ns at NPT (Isothermal-Isobaric ensemble, constant temperature, pressure, and the number of particles) ensemble temperature of 300k and 1.01325 bar of pressure. The Desmond simulation interaction diagram tool of Maestro was used to generate the simulation interaction diagram. root-mean-square deviation (RMSD), root mean square fluctuation (RMSF), number of H-bonds, total contacts timeline and Protein-Ligand interactions were recorded throughout the simulation data and were analyzed to validate our findings in molecular docking.

3.5. Molecular Mechanics Generalized Born Surface Area (MM-GBSA) Calculations:

The binding free energy calculation of the protein-ligand docking complexes was estimated by using the Prime-MM/GBSA by using OPLS2005 force field [49, 50, 30] by using the methods described in previously published manuscript [51]. Prime MM-GBSA method calculates the binding free energy as follows:

$$\Delta G_{binding} = G_{docking\ complex} - (G_{protein} + G_{ligand})$$

Where, $\Delta G_{binding}$ = total binding free energy, $G_{docking\ complex}$, $G_{protein}$, and G_{ligand} are the free energies of the docking complex, protein and ligand, respectively. The obtained results were presented as the mean ± standard deviation (SD).

3.6. Dynamic Cross-Correlation Matrix (DCCM) and Principal Component Analysis (PCA) of the MD Simulation Trajectories

In order to analyze the domain correlations dynamic cross-correlation matrix (DCCM) were generated across all Cα-atoms for Macrolactin A and 6LU7 complex during the MD simulation of 100 ns. PCA analysis was performed to extract the fast and slow motions of the trajectories during 100 ns simulation of 6LU7 complexed with Macrolactin A. A covariance matrix was generated to calculate the PCA for global slow motion and local fast motion of the contributing amino acid residues from each MD trajectory as described elsewhere [31]. The DCCM and PCA analyses were done using trj_essential_dynamics script of Schrodinger [34, 35, 48].

4. Conclusions

Virtual screening of 30 natural compounds resulted in the identification of Macrolactin A as a lead compound for further *in-vitro* and *in-vivo* studies and ultimately as a treatment of Covid-19. Macrolactin A showed a very good docking score of -9.22 kcal/mol and formed 3 hydrogen bonds and several other interactions. ADME revealed that it possesses favorable physicochemical properties and good drug-likeness scores. MD simulations showed that bounds in M^{pro}-Macrolactin A complex were strong and stable throughout 100ns. MM-GBSA analysis showed ΔGbind of -42.58 kcal/mol. Contacts timeline analysis of Macrolactin A showed that HIS 41, ASN 142, TYR 154, GLU 166, and GLN 189 were the crucial interactions. However, slight modification via derivatization might be required to improve its percentage human oral. Overall, Macrolactin A was the most promising compound to be used against SARS-CoV-2. This compound is produced by soil bacteria *Bacillus amyloliquefaciens* and was first isolated in 1989 [30]. This could make producing this compound on an industrial scale very easy and cost-effective due to the ease of culturing *bacillus* species. It has been previously reported to possess strong antifungal [52] and antibacterial activity even against vancomycin-resistant enterococci and methicillin-resistant *Staphylococcus aureus* [53]. It has also been fully synthesized which make it even more accessible to the world [54].

Supplementary Materials: The following are available online, Table S1. List of Total Molecules with their sources, PDB, and activities; Table S2. Lipinski Filtered compounds with molecular properties. Table S3. Binding energies (kcal/mol) of selected natural bioactive compounds with M^{pro} and their interactions with the binding site amino acid residues. Fig S1. Docking of 14 compound; Fig S2. Analysis of total contacts timeline formed between M^{pro} protein residues and Stachyflin during MD simulation. Darker shades correspond to a higher number of contacts and Stachyflin.

Author Contributions: Conceptualization, S.P., T.S., K.K.B., and M.K.P..; methodology, K.K.B., S.P., A.G., B.R., and D.B.; formal analysis, T.S., K.K.B B.R., and A.G.; investigation S.P., T.S., K.K.B., and M.K.P.; writing—original draft preparation, K.K.B.,S.P., H.I.S.,B.P.D. and B.R.N.; writing—review and editing, D.B.,A.G., S.S.,A.J. and H.A.E.,. All authors have read and agreed to the published version of the manuscript.

Conflicts of interest: The authors declare no conflicts of interest.

References:

(1) Lee, N.; Allen Chan, K. C.; Hui, D. S.; Ng, E. K. O.; Wu, A.; Chiu, R. W. K.; Wong, V. W. S.; Chan, P. K. S.; Wong, K. T.; Wong, E.; Cockram, C. S.; Tam, J. S.; Sung, J. J. Y.; Lo, Y. M. D. Effects of Early Corticosteroid Treatment on Plasma SARS-Associated Coronavirus RNA Concentrations in Adult Patients. *J. Clin. Virol.* **2004**, *31* (4), 304–309. https://doi.org/https://doi.org/10.1016/j.jcv.2004.07.006.

(2) de Groot, R. J.; Baker, S. C.; Baric, R. S.; Brown, C. S.; Drosten, C.; Enjuanes, L.; Fouchier, R. A. M.; Galiano, M.; Gorbalenya, A. E.; Memish, Z. A.; Perlman, S.; Poon, L. L. M.; Snijder, E. J.; Stephens, G. M.; Woo, P. C. Y.; Zaki, A. M.; Zambon, M.; Ziebuhr, J. Middle East Respiratory Syndrome Coronavirus (MERS-CoV): Announcement of the Coronavirus Study Group. *J. Virol.* **2013**, *87* (14), 7790–7792. https://doi.org/10.1128/JVI.01244-13.

(3) Worldometer. Coronavirus Update (Live)_ 7,405,051 Cases and 416,626 Deaths from COVID-19 Virus Pandemic - Worldometer.

(4) Gautret, P.; Lagier, J. C.; Parola, P.; Hoang, V. T.; Meddeb, L.; Mailhe, M.; Doudier, B.; Courjon, J.; Giordanengo, V.; Vieira, V. E.; Tissot Dupont, H.; Honoré, S.; Colson, P.; Chabrière, E.; La Scola, B.; Rolain, J. M.; Brouqui, P.; Raoult, D. Hydroxychloroquine and Azithromycin as a Treatment of COVID-19: Results of an Open-Label Non-Randomized Clinical Trial. *Int. J. Antimicrob. Agents* **2020**. https://doi.org/10.1016/j.ijantimicag.2020.105949.

(5) Lu, R.; Zhao, X.; Li, J.; Niu, P.; Yang, B.; Wu, H.; Wang, W.; Song, H.; Huang, B.; Zhu, N.; Bi, Y.; Ma, X.; Zhan, F.; Wang, L.; Hu, T.; Zhou, H.; Hu, Z.; Zhou, W.; Zhao, L.; Chen, J.; Meng, Y.; Wang, J.; Lin, Y.; Yuan, J.; Xie, Z.; Ma, J.; Liu, W. J.; Wang, D.; Xu, W.; Holmes, E. C.; Gao, G. F.; Wu, G.; Chen, W.; Shi, W.; Tan, W. Genomic Characterisation and Epidemiology of 2019 Novel Coronavirus: Implications for Virus Origins and Receptor Binding. *Lancet* **2020**, *395* (10224), 565–574. https://doi.org/10.1016/S0140-6736(20)30251-8.

(6) Kumaravel, S. K.; Subramani, R. K.; Jayaraj Sivakumar, T. K.; Madurai Elavarasan, R.; Manavalanagar Vetrichelvan, A.; Annam, A.; Subramaniam, U. Investigation on the Impacts of COVID-19 Quarantine on Society and Environment: Preventive Measures and Supportive Technologies. *3 Biotech* **2020**, *10* (9), 393. https://doi.org/10.1007/s13205-020-02382-3.

(7) Elena, S. F.; Sanjuán, R. Adaptive Value of High Mutation Rates of RNA Viruses: Separating Causes from Consequences. *J. Virol.* **2005**, *79* (18), 11555 LP – 11558. https://doi.org/10.1128/JVI.79.18.11555-11558.2005.

(8) Sahin, A. R.; Erdogan, A.; Agaoglu, P. M.; Dineri, Y.; Cakirci, A. Y.; Senel, M. E.; Okyay, R. .; Tasdogan, A. M. 2019 Novel Coronavirus

(COVID-19) Outbreak: A Review of the Current Literature. *EURASIAN J. Med. Oncol.* **2020**, *4* (1), 1–7.
(9) Cao, B.; Wang, Y.; Wen, D.; Liu, W.; Wang, J.; Fan, G.; Ruan, L.; Song, B.; Cai, Y.; Wei, M.; Li, X.; Xia, J.; Chen, N.; Xiang, J.; Yu, T.; Bai, T.; Xie, X.; Zhang, L.; Li, C.; Yuan, Y.; Chen, H.; Li, H.; Huang, H.; Tu, S.; Gong, F.; Liu, Y.; Wei, Y.; Dong, C.; Zhou, F.; Gu, X.; Xu, J.; Liu, Z.; Zhang, Y.; Li, H.; Shang, L.; Wang, K.; Li, K.; Zhou, X.; Dong, X.; Qu, Z.; Lu, S.; Hu, X.; Ruan, S.; Luo, S.; Wu, J.; Peng, L.; Cheng, F.; Pan, L.; Zou, J.; Jia, C.; Wang, J.; Liu, X.; Wang, S.; Wu, X.; Ge, Q.; He, J.; Zhan, H.; Qiu, F.; Guo, L.; Huang, C.; Jaki, T.; Hayden, F. G.; Horby, P. W.; Zhang, D.; Wang, C. A Trial of Lopinavir–Ritonavir in Adults Hospitalized with Severe Covid-19. *N. Engl. J. Med.* **2020**, *382* (19), 1787–1799. https://doi.org/10.1056/nejmoa2001282.
(10) Wang, N.; Shang, J.; Jiang, S.; Du, L. Subunit Vaccines Against Emerging Pathogenic Human Coronaviruses. *Frontiers in Microbiology*. 2020. https://doi.org/10.3389/fmicb.2020.00298.
(11) Lin, L. T.; Hsu, W. C.; Lin, C. C. Antiviral Natural Products and Herbal Medicines. *J. Tradit. Complement. Med.* **2014**, *4* (1), 24–35.
(12) Harvey, A. L.; Edrada-Ebel, R.; Quinn, R. J. The Re-Emergence of Natural Products for Drug Discovery in the Genomics Era. *Nat. Rev. drug Discov.* **2015**, *14* (2), 111–129.
(13) Reeves, J. D.; Piefer, A. J. Emerging Drug Targets for Antiretroviral Therapy. *Drugs* **2005**, *65* (13), 1747–1766.
(14) Chen, X.; Ung, C. Y.; Chen, Y. Can an in Silico Drug-Target Search Method Be Used to Probe Potential Mechanisms of Medicinal Plant Ingredients? *Nat. Prod. Rep.* **2003**, *20* (4), 432–444.
(15) Gorgulla, C.; Boeszoermenyi, A.; Wang, Z. F.; Fischer, P. D.; Coote, P. W.; Das, K. M. P.; Malets, Y. .; Radchenko, D. .; Moroz, Y. .; Scott, D. .; Fackeldey, K. An Open-Source Drug Discovery Platform Enables Ultra-Large Virtual Screens. , . *Nature* **2020**, *580* (7805), 663–668.
(16) Adejoro, I. A.; Babatunde, D. D.; Tolufashe, G. F. Molecular Docking and Dynamic Simulations of Some Medicinal Plants Compounds against SARS-CoV-2: An in Silico Study. *J. Taibah Univ. Sci.* **2020**, *14* (1), 1563–1570.
(17) Rajagopal, K.; Varakumar, P.; Baliwada, A.; Byran, G. Activity of phytochemical constituents of Curcuma longa (turmeric) and Andrographis paniculata against coronavirus (COVID-19): An in silico approach. Future J. Pharm. Sci. 2020, 6, 104.

(18) Chen, J.; Liu, T.; Wei, M.; Zhu, Z.; Liu, W.; Zhang, Z. Macrolactin a Is the Key Antibacterial Substance of Bacillus Amyloliquefaciens D2WM against the Pathogen Dickeya Chrysanthemi. *Eur. J. Plant Pathol.* **2019**, *155* (2), 393–404. https://doi.org/10.1007/s10658-019-01774-3.
(19) Gustafson, K.; Roman, M.; Fenical, W. The Macrolactins, a Novel Class of Antiviral and Cytotoxic Macrolides from a Deep-Sea Marine Bacterium. *J. Am. Chem. Soc.* **1989**, *111* (19), 7519–7524. https://doi.org/10.1021/ja00201a036.
(20) Kim, E.-N.; Gao, M.; Choi, H.; Jeong, G.-S. Marine Microorganism-Derived Macrolactins Inhibit Inflammatory Mediator Effects in LPS-Induced Macrophage and Microglial Cells by Regulating BACH1 and HO-1/Nrf2 Signals through Inhibition of TLR4 Activation. *Molecules* **2020**, *25* (3), 656. https://doi.org/10.3390/molecules25030656.
(21) Joshi, R. S.; Jagdale, S. S.; Bansode, S. B.; Shankar, S. S.; Tellis, M. B.; Pandya, V. K.; Chugh, A.; Giri, A. P.; Kulkarni, M. J. Discovery of Potential Multi-Target-Directed Ligands by Targeting Host-Specific SARS-CoV-2 Structurally Conserved Main Protease. *J. Biomol. Struct. Dyn.* **2020**, 1–16. https://doi.org/10.1080/07391102.2020.1760137.
(22) Enmozhi, S. K.; Raja, K.; Sebastine, I.; Joseph, J. Andrographolide as a Potential Inhibitor of SARS-CoV-2 Main Protease: An in Silico Approach. *J. Biomol. Struct. Dyn.* **2020**, 1–7. https://doi.org/10.1080/07391102.2020.1760136.
(23) Das, S.; Sarmah, S.; Lyndem, S.; Singha Roy, A. An Investigation into the Identification of Potential Inhibitors of SARS-CoV-2 Main Protease Using Molecular Docking Study. *J. Biomol. Struct. Dyn.* **2020**, 1–11. https://doi.org/10.1080/07391102.2020.1763201.
(24) Bharadwaj, S.; Azhar, E. I.; Kamal, M. A.; Bajrai, L. H.; Dubey, A.; Jha, K.; Yadava, U.; Kang, S. G.; Dwivedi, V. D. SARS-CoV-2 Mpro Inhibitors: Identification of Anti-SARS-CoV-2 Mpro Compounds from FDA Approved Drugs. *J. Biomol. Struct. Dyn.* **2020**, 1–16. https://doi.org/10.1080/07391102.2020.1842807.
(25) Tiwari, V. Novel Hybrid Antiviral VTRRT-13V2.1 against SARS-CoV2 Main Protease: Retro-Combinatorial Synthesis and Molecular Dynamics Analysis. *Heliyon* **2020**, *6* (10), e05122. https://doi.org/https://doi.org/10.1016/j.heliyon.2020.e05122.
(26) Prasanth, D. S. N. B. K.; Murahari, M.; Chandramohan, V.; Panda, S. P.; Atmakuri, L. R.; Guntupalli, C. In Silico Identification of Potential Inhibitors from Cinnamon against Main Protease and Spike Glycoprotein of SARS CoV-2. *J. Biomol. Struct. Dyn.* **2020**, 1–15.
(27) Vivek-Ananth, R. P.; Rana, A.; Rajan, N.; Biswal, H. S.; Samal, A. In Silico Identification of Potential Natural Product Inhibitors of Human Proteases Key to SARS-CoV-2 Infection. *arXiv Prepr. arXiv2006.00652.* **2020**.
(28) Juárez-Saldívar, A.; Lara-Ramírez, E. E.; Reyes-Espinosa, F.; Paz-González, A. D.; Villalobos-Rocha, J. C.; Rivera, G. Ligand-Based and Structured-Based In Silico Repurposing Approaches to Predict Inhibitors of SARS-CoV-2 Mpro Protein. *Scientia Pharmaceutica* . 2020. https://doi.org/10.3390/scipharm88040054.
(29) Mondal, P.; Natesh, J.; Abdul Salam, A. A.; Thiyagarajan, S.; Meeran, S. M. Traditional Medicinal Plants against Replication, Maturation and Transmission Targets of SARS-CoV-2: Computational Investigation. *J. Biomol. Struct. Dyn.* **2020**, 1–18. https://doi.org/10.1080/07391102.2020.1842246.
(30) Choudhary, M. I.; Shaikh, M.; Tul-Wahab, A.; Ur-Rahman, A. In Silico Identification of Potential Inhibitors of Key SARS-CoV-2 3CL Hydrolase (Mpro) via Molecular Docking, MMGBSA Predictive Binding Energy Calculations, and Molecular Dynamics Simulation. *PLoS One* **2020**, *15* (7), e0235030.
(31) Piao, L.; Chen, Z.; Li, Q.; Liu, R.; Song, W.; Kong, R.; Chang, S. Molecular Dynamics Simulations of Wild Type and Mutants of SAPAP in Complexed with Shank3. *International Journal of Molecular Sciences* . 2019. https://doi.org/10.3390/ijms20010224.
(32) Lipinski, C. A. Drug-like Properties and the Causes of Poor Solubility and Poor Permeability. *J. Pharmacol. Toxicol. Methods* **2000**, *44* (1), 235–249. https://doi.org/https://doi.org/10.1016/S1056-8719(00)00107-6.
(33) Lipinski, C. A.; Lombardo, F.; Dominy, B. W.; Feeney, P. J. Experimental and Computational Approaches to Estimate Solubility and Permeability in Drug Discovery and Development Settings1PII of Original Article: S0169-409X(96)00423-1. The Article Was Originally Published in Advanced Drug Delivery Reviews 23 (1997) 3. *Adv. Drug Deliv. Rev.* **2001**, *46* (1), 3–26. https://doi.org/https://doi.org/10.1016/S0169-409X(00)00129-0.
(34) Schrödinger. Qikprop 4.4 User Manual. 2015.
(35) Schrodinger Release 2020–2: QikProp, LLC. New York, NY 2020.
(36) Duffy, E. M.; Jorgensen, W. L. Prediction of Properties from Simulations: Free Energies of Solvation in Hexadecane, Octanol, and Water. *J. Am. Chem. Soc.* **2000**, *122* (12), 2878–2888. https://doi.org/10.1021/ja993663t.
(37) Jorgensen, W. L.; Duffy, E. M. Prediction of Drug Solubility from Monte Carlo Simulations. *Bioorg. Med. Chem. Lett.* **2000**, *10* (11), 1155–1158. https://doi.org/https://doi.org/10.1016/S0960-894X(00)00172-4.
(38) Jorgensen, W. L.; Duffy, E. M. Prediction of Drug Solubility from Structure. *Adv. Drug Deliv. Rev.* **2002**, *54* (3), 355–366. https://doi.org/https://doi.org/10.1016/S0169-409X(02)00008-X.
(39) Schrodinger Release 2020–1: LigPrep, LLC. New York, NY 2020.

(40) Schrödinger Suite 2020: Protein Preparation Wizard, LLC. New York, NY 2020.
(41) Harder, E.; Damm, W.; Maple, J.; Wu, C.; Reboul, M.; Xiang, J. Y.; Wang, L.; Lupyan, D.; Dahlgren, M. K.; Knight, J. L.; Kaus, J. W.; Cerutti, D. S.; Krilov, G.; Jorgensen, W. L.; Abel, R.; Friesner, R. A. OPLS3: A Force Field Providing Broad Coverage of Drug-like Small Molecules and Proteins. *J. Chem. Theory Comput.* **2016**, *12* (1), 281–296. https://doi.org/10.1021/acs.jctc.5b00864.
(42) Jin, Z.; Du, X.; Xu, Y.; Deng, Y.; Liu, M.; Zhao, Y.; Zhang, B.; Li, X.; Zhang, L.; Peng, C.; Duan, Y.; Yu, J.; Wang, L.; Yang, K.; Liu, F.; Jiang, R.; Yang, X.; You, T.; Liu, X.; Yang, X.; Bai, F.; Liu, H.; Liu, X.; Guddat, L. W.; Xu, W.; Xiao, G.; Qin, C.; Shi, Z.; Jiang, H.; Rao, Z.; Yang, H. Structure of Mpro from SARS-CoV-2 and Discovery of Its Inhibitors. *Nature* **2020**, *582* (7811), 289–293. https://doi.org/10.1038/s41586-020-2223-y.
(43) Jacobson, M. P.; Pincus, D. L.; Rapp, C. S.; Day, T. J. F.; Honig, B.; Shaw, D. E.; Friesner, R. A. A Hierarchical Approach to All-Atom Protein Loop Prediction. *Proteins Struct. Funct. Bioinforma.* **2004**, *55* (2), 351–367. https://doi.org/https://doi.org/10.1002/prot.10613.
(44) Forli, S.; Huey, R.; Pique, M. E.; Sanner, M. F.; Goodsell, D. S.; Olson, A. J. Computational Protein–Ligand Docking and Virtual Drug Screening with the AutoDock Suite. *Nat. Protoc.* **2016**, *11* (5), 905–919. https://doi.org/10.1038/nprot.2016.051.
(45) Morris, G. M.; Huey, R.; Lindstrom, W.; Sanner, M. F.; Belew, R. K.; Goodsell, D. S.; Olson, A. J. AutoDock4 and AutoDockTools4: Automated Docking with Selective Receptor Flexibility. *J. Comput. Chem.* **2009**, *30* (16), 2785–2791. https://doi.org/https://doi.org/10.1002/jcc.21256.
(46) Bikadi, Z.; Hazai, E. Application of the PM6 Semi-Empirical Method to Modeling Proteins Enhances Docking Accuracy of AutoDock. *J. Cheminform.* **2009**, *1* (1), 15. https://doi.org/10.1186/1758-2946-1-15.
(47) Biovia, D. BIOVIA Discovery Studio 2017 R2: A Comprehensive Predictive Science Application for the Life Sciences. BIOVIA Discovery Studio 2017.
(48) Schrödinger Release 2020–1: Desmond Molecular Dynamics System, D. E. Shaw Research, Maestro-Desmond Interoperability Tools. New York, NY 2020.
(49) Prime, Schrödinger, LLC. 2020.
(50) Schrödinger Suite 2020: Prime, Version 3.1. LLC. New York, NY 2020.
(51) Lee, K. E.; Bharadwaj, S.; Yadava, U.; Kang, S. G. Computational and In Vitro Investigation of (-)-Epicatechin and Proanthocyanidin B2 as Inhibitors of Human Matrix Metalloproteinase 1. *Biomolecules* **2020**, *10* (10). https://doi.org/10.3390/biom10101379.
(52) Salazar, F.; Ortiz, A.; Sansinenea, E. A Strong Antifungal Activity of 7-O-Succinyl Macrolactin A vs Macrolactin A from Bacillus Amyloliquefaciens ELI149. *Curr. Microbiol.* **2020**, *77* (11), 3409–3413. https://doi.org/10.1007/s00284-020-02200-2.
(53) Kim, D. H.; Kim, H. K.; Kim, K. M.; Kim, C. K.; Jeong, M. H.; Ko, C. Y.; Moon, K. H.; Kang, J. S. Antibacterial Activities of Macrolactin a and 7-O-Succinyl Macrolactin a from Bacillus Polyfermenticus KJS-2 against Vancomycin-Resistant Enterococci and Methicillin-Resistant Staphylococcus Aureus. *Arch. Pharm. Res.* **2011**, *34* (1), 147–152. https://doi.org/10.1007/s12272-011-0117-0.
(54) Smith, A.; Ott, G. Total Synthesis of (−)-Macrolactin A. *J. Am. Chem. Soc.* **1996**, *118* (51), 13095–13096.